Experimental Investigation of a New Two-Microphone Method for the Determination of Broadband Noise Radiation from Ducts

Jonathan Melling, Jian Chen and Phillip Joseph

Institute of Sound and Vibration Research, University of Southampton, Southampton SO17 1BJ, UK

Abstract

This paper experimentally investigates a new technique for measuring the modal amplitude distribution, sound power transmission and radiation, and far field directivity of the broadband noise from hard walled ducts. The innovative aspect of this method is that it only requires the measurements of the two-point complex coherence function between the acoustic pressures at two closely spaced points on the duct wall. This method is therefore very useful when direct measurements of sound power and directivity are not possible. This paper describes detailed measurements of the sound power spectrum and coherence function from a hard walled circular duct excited at one end by a diffuse sound field. The other open end is terminated within an anechoic chamber with which to measure the radiated sound field at 11 microphones distributed over a polar arc. Measurements of the complex coherence were made at the duct and used to infer the sound power spectrum and far field directivity. This paper demonstrates generally good agreement between direct measurements of sound power and directivity and those inferred from the coherence function. The method is restricted to broadband noise in large ducts in the frequency range where many modes are able to propagate and the modal amplitudes are mutually uncorrelated.

Keywords: duct acoustics, modal amplitude distribution, complex coherence, far field directivity, sound power radiation

Nomenclature

a	=	Duct radius
$\overline{a_{\pm}^2}$	=	Normalised mean square mode amplitude distribution for positive and negative propagating modes
c	=	Speed of sound
f_{sch}	=	Schroeder frequency
k	=	Acoustic wavenumber
p	=	Acoustic pressure
x_D	=	Distance along duct of measurement
Δx	=	In-duct microphone separation distance
A	=	Duct area
A_{mn}	=	Pressure amplitude of mode

L	=	Length of duct
N	=	Total number of propagating modes at a particular frequency
$\left\|R_r(\omega)\right\|^2$	=	Energy reflection coefficient
R	=	Far-field radial position from centre of the duct
S_{11}	=	Pressure Power Spectral Density at the duct wall
S_{12}	=	Pressure Cross Spectral Density at the duct wall
S_{ff}	=	Pressure Power Spectral Density of far-field radiation
$S(\omega)$	=	Frequency-dependent source strength
$\left\|T(\omega)\right\|^2$	=	Energy transmission coefficient
T_{60}	=	Reverberation time
V	=	Source room volume
$W(\omega)$	=	Transmitted power
α	=	Cuton ratio
θ	=	Polar co-ordinate of far-field observer
ρ	=	Density of air
ω	=	Angular frequency
$\hat{\omega}$	=	Non-dimensional frequency
ψ_{12}	=	Complex coherence function
Ω^+	=	Sound power factors
$\Gamma(\hat{\omega})$	=	Hanning window function

1. Introduction

Ducts, also known as waveguides, are able to efficiently transmit noise over large distances, which may then radiate from the end of the duct. Common examples are ventilation/exhaust ducts, automotive silencers, and turbofan aero-engines. Often one wishes to determine the far field directivity and sound power radiating from the duct open end, either as an index of transmission loss to assess the performance of silencer, or as a means of scaling the total noise level for predicting community noise annoyance.

In the case of an exhaust duct and a turbofan engine, for example, locating microphones in the far field is difficult. In the case of turbofan engines very large anechoic facilities are needed. Without these facilities, therefore, an alternative technique the far-field directivity and sound power may be inferred from in-duct acoustic pressure measurements. In-duct measurement techniques have been developed using microphone arrays to localise the broadband sources in the duct [1-3] using acoustic imaging methods, such as beamforming. Measurement techniques have also been developed to

estimate the far-field directivity from acoustic pressure measurements made on the duct wall based on a decomposition of the sound field into its propagating modal components. The amplitudes of each mode are first determined by a microphone phased array. Next the pattern of individual mode propagating to the far-field is predicted by the amplitude of the corresponding in-duct mode.

Measurement techniques for the modal decomposition of tonal noise in the duct has been developed in the early 1970's [4] by inverting a matrix of modal response functions based on a modal propagation model. The modal decomposition of broadband noise is more problematic however since the mode amplitudes are partially coherent and all modes are potentially excited. In a typical aero-engine duct, for example, the number of propagating modes can easily exceed 100 at the blade passing frequency. One current method to determine the amplitude of each mode requires a large microphone array in the duct comprising many rings of microphones. In general, at least as many microphones as modes are required to deduce all mode amplitudes. Researchers at Boeing [5] developed a circumferential row array with a large number of microphones to evaluate sound pressure as a function of azimuthal wavenumber or spinning mode order. Later, researchers at Boeing [6] designed more sophisticated ring arrays in the inlet, inter-stage and bypass sections of an aero-engine duct to decompose the acoustic pressure at the wall sound pressure level into spinning modes. However, neither work attempted to relate the in-duct modal decomposition to the far-field sound radiation. Enghardt et al. [7, 8] has recently proposed an in-duct measurement technique to decompose the broadband sound field into its constituent modes at a maximum frequency corresponding to about 150 propagating modes. No attempt was made to predict the far field radiation, however. Another method [9] is based on an axial array of microphones along the duct wall. Conventional beamforming was applied to the array to estimate the mode amplitude distribution versus the modal propagation angle, which was then used to infer both the total sound power and far field directivity. However, this method requires many microphones arranged along a long length of duct (many acoustic wavelengths).

As mentioned above, using large arrays of microphones have the disadvantage that they occupy a large space, which is not always available as well as being costly since it requires good quality microphones with stable phase characteristics as well as a data acquisition system comprising a large number of channels. To overcome these difficulties a new method has recently been developed by Joseph et al. [10, 11] in which the mode amplitude distribution, transmitted and radiated sound power, and far field directivity can be estimated from measurements of only the complex coherence function between the acoustic pressure at two closely spaced positions at the duct wall. The method makes a number of crucial assumptions about the sound field, which have so far *not* been validated experimentally. This paper presents an experimental investigation into the accuracy and validity of this two microphone method and validate experimentally some of the main simplifying assumptions behind the technique.

2. Measurement theory

Before discussing the experimental method and measurement procedure we first outline the theory underlying the measurement principle. A fuller derivation of the underlying theory is presented in the Appendix and the detailed theoretical development presented in [Ref 10, https://www.acoustics.asn.au/conference_proceedings/INTERNOISE2014/papers/p949.pdf].

2.1 Mode amplitude distribution

The theory in Ref. [10] includes the effects of a uniform mean flow. Here the effects of flow are ignored for consistency with the no-flow measurements presented in Sections 3 and 4.

Above its cutoff frequency, at a single (angular) frequency ω, a single mode propagating along the duct of pressure amplitude A_{mn} is described by

$$p^{\pm}_{mn}(\boldsymbol{y},x) = \mathrm{e}^{-\mathrm{i}\omega t} A^{\pm}_{mn} \Psi_{mn}(\boldsymbol{y}) \mathrm{e}^{\pm \mathrm{i}\alpha_{mn} k x} \tag{1}$$

In this equation the superscript "+" and "-" refers to the modes propagating in the positive (away from the source) and negative x directions (towards the source), respectively, m and n denote the usual mode indices of the propagating azimuthal mode and radial mode respectively, $\boldsymbol{y} = (r,\theta)$ is a position vector on the duct cross sectional area with radial and azimuthal coordinates r and θ, $\Psi_{mn}(\boldsymbol{y})$ denotes the modal shape function with the normalisation property, $A^{-1}\int_A |\Psi_{mn}(\boldsymbol{y})|^2 \,\mathrm{d}A(\boldsymbol{y}) = 1$ where A is the duct cross sectional area, and $k = \omega/c$ is the free space wavenumber and c is the sound speed. Of central importance in Eq. (1) is the parameter α_{mn}, which we shall call the modal cut-on ratio, given by,

$$\alpha_{mn} = \sqrt{1-(\kappa_{mn}/k)^2} \tag{2}$$

where κ_{mn} is a set of eigenvalues that are characteristic of the duct cross section such that the corresponding mode shape functions Ψ_{mn}, defined by $(\nabla^2_{\perp} + \kappa^2_{mn})\Psi_{mn}(\boldsymbol{y}) = 0$, also satisfy the duct-wall boundary conditions. In a hard wall duct, κ_{mn} takes the values $\kappa_{mn} = j'_{mn}/a$ where j'_{mn} denotes the n^{th} stationary value of the Bessel function of order m. The cut-on ratio α_{mn} is central in what follows and takes values between $\alpha_{mn} = 0$ precisely at the modal cutoff frequency $\omega = \omega_{mn} = \kappa_{mn} c$, and tends to $\alpha_{mn} = 1$ as $\omega/\omega_{mn} \to \infty$, corresponding to modes well above cuton.

The significance of the cuton ratio to duct acoustics, or its related quantity cuton ratio $\left(1-\alpha_{mn}^{\ 2}\right)^{-1}=k/\kappa$, was highlighted in the work of Rice [12] and Joseph et al. [13]. It is an important quantity in duct acoustics since different modes with the same cuton ratio have similar transmission and radiation characteristics, Rice [12]. Cuton ratio is uniquely related to the angle θ_{mn} through $\alpha_{mn}=\cos\theta_{mn}$ [14], with which the mode propagates along the duct relative to the axis. It has also been shown that θ_{mn} equals to the angle radiated most strongly to the far field (the angle of the main lobe), Rice [12]. Lastly, it has been shown that the mode amplitude distribution for many physical source distributions is a smoothly varying function of α_{mn}.

2.2 Simplifying assumptions

To develop the main theoretical relationships underlying the measurement principle investigated in this paper, we further make the following simplifying assumptions about the multi-mode broadband sound field:

(1) Mode amplitudes are statistically uncorrelated.

(2) The mean square pressure mode amplitude $A_{mn}^{\pm}$ in Eq. (1) can be written in the separable form,

$$E\left\{\left|A_{mn}^{\pm}(\omega)\right|^2\right\}=S(\omega)\overline{a_{\pm}^2}(\alpha_{mn}) \tag{3}$$

where $S(\omega)$ is a frequency-dependent source term and $\overline{a_{\pm}^2}(\alpha_{mn})$ is a normalised, non-dimensional, frequency-independence mode amplitude distribution function of the cuton ratio α. The separability assumption of Eq. (3) is met. Rice [12] and more recently Joseph et al. [10] have shown that this is a valid assumption for a broad class of physically important mode amplitude distribution functions such as spatial distributions of monopoles, dipoles and the case where each mode has identical energy.

(3) The excitation frequency is sufficiently high to ensure that there are a sufficient number of modes so that its distribution versus α may be approximated as a continuous function. This is believed to be correct for $ka>10$, where a is the duct radius.

2.3 Fourier Transform relation between mode amplitude distribution and wall pressure coherence function

By applying the simplifying assumptions listed above, in the Appendix we derive a Fourier Transform relationship between the mean square mode amplitude distribution $\overline{a^2}(\alpha)$ as a function of α and the complex coherence function $\psi_{12}(\hat{\omega})$

$$\psi_{12}(\hat{\omega}) = \int_{-1}^{+1} \overline{a^2}(\alpha)|\alpha| e^{-i\hat{\omega}\alpha} d\alpha \quad , \quad \overline{a^2}(\alpha) = \frac{1}{2\pi|\alpha|} \int_{0}^{\infty} \psi_{12}(\hat{\omega}) e^{i\hat{\omega}\alpha} d\hat{\omega} \tag{4a, b}$$

where $\hat{\omega}$ is the non-dimensional frequency $\hat{\omega} = \omega \Delta x / c$, α now varies between -1 and 1, such that the positive and negative going mode amplitude distribution, $\overline{a_{\pm}^2}(\alpha_{mn})$, in Eq. (3) is replaced by a single distribution $\overline{a^2}(\alpha)$ with positive-going modes identified by positive α values and negative going modes identified with negative values of α, i.e,

$$\begin{aligned} \overline{a^2}(\alpha) &= \overline{a_+^2}(\alpha) \qquad (\alpha \geq 0) \\ \overline{a^2}(\alpha) &= \overline{a_-^2}(-\alpha) \qquad (\alpha \leq 0) \end{aligned} \tag{5}$$

and the complex coherence function $\psi_{12}(\hat{\omega})$ is defined by

$$\psi_{12}(\hat{\omega}) = \frac{S_{12}(\hat{\omega})}{\sqrt{S_{11}(\hat{\omega}) S_{22}(\hat{\omega})}} \qquad \left(0 \leq |\psi_{12}(\hat{\omega})|^2 \leq 1\right) \tag{6}$$

where $S_{12}(\hat{\omega})$ is the acoustic pressure Cross Spectrum Density (CSD) between the two measurement positions, and $S_{11}(\hat{\omega})$ and $S_{22}(\hat{\omega})$ are the acoustic pressure Power Spectral Densities (PSD) measured at the two microphones.

Note that, whilst Eqs. (4a and b) were derived for circular hard walled duct, it is completely general and applies to all hard walled prismatic ducts since in their derivation the modal shape functions are replaced by their average values at the duct wall.

2.4 Far field directivity

Knowledge of the mode amplitude distribution versus α is sufficient to determine the PSD, $S_{ff}(\omega,\theta)$, of the far field sound pressure radiated from the open end of the duct versus polar radiation angle θ

measured relative to the duct axis [12, 13]. In the absence of flow the cuton ratio α is related to the propagation angle through $\alpha = \cos\theta$. Using this result and that the angle of the main radiation lobe of far field directivity equals θ, in Ref. [12], it is shown in Ref. [10] that $S_{ff}(\omega,\theta)$ can be deduced from the coherence function $\psi_{12}(\hat{\omega})$ from the equation,

$$\frac{S_{ff}(\omega,\theta)}{S_{11}(\omega)} = \mathrm{d}(\theta), \quad (0 \le \theta \le \pi/2) \tag{7}$$

where $\mathrm{d}(\theta)$ is the non-dimensional frequency-independent directivity function

$$\mathrm{d}(\theta) = \frac{1}{8\pi}\left(\frac{a}{R}\right)^2 \cos\theta \int_0^\infty \psi_{12}(\hat{\omega}) \mathrm{e}^{-\mathrm{i}\hat{\omega}\cos\theta} \mathrm{d}\hat{\omega} \tag{8}$$

The expression on the right hand side of Eq. (8) is an integral over $\hat{\omega}$ and therefore the normalised directivity function is predicted to be independent of frequency, which is a consequence of making the separability assumption of Eq. (3).

2.5 Sound power radiation

The mode amplitude distribution versus α is sufficient to determine exactly the sound power transmitted along the duct for both positive W^+ and negative going set of modes W^-. Joseph et al. [10] has shown that the sound power transmitted may be computed directly from the complex coherence function. In the absence of flow, the result in Ref. [10] reduces to,

$$\frac{4\pi W^{\pm}(\omega)\rho c}{S_{11}(\omega)A} = \varpi^{\pm} \tag{9}$$

where $\varpi^{\pm}$ is a frequency-independent constant factor determined from the coherence function, according to

$$\varpi^{\pm} = \int_0^\infty \psi_{12}(\hat{\omega}) \Omega^{\pm}(\hat{\omega}) \mathrm{d}\hat{\omega} \tag{10}$$

In the absence of flow and reflections, sound power is transmitted from left to right away from the source and $\Omega^+(\hat{\omega})$ is given by,

$$\Omega^+(\hat{\omega}) = \frac{\mathrm{e}^{\mathrm{i}\hat{\omega}}(1-\mathrm{i}\hat{\omega}) - 1}{\hat{\omega}^2} \tag{11}$$

The far field directivity and transmitted (and hence radiated) sound powers will be estimated in Sections 2.4 and 2.5 from Eqs. (7) and (8) respectively using coherence measurements made on the wall of a rigid walled duct excited at one end by a diffuse sound field. The estimates will be compared against direct measurements of directivity and radiated sound power by way of validation of this new two-microphone method.

3. Experimental methodology

This section describes the experimental arrangement used to validate the measurement theory outlined in Section 2. In order to validate this new measurement technique, acoustic pressure measurements were made of the broadband sound field at two closely spaced positions on the wall of the duct and at 11 microphones in the far field of the duct open end. Complex coherence measurements made at the two duct wall positions were used in Eqs. (7, 8) and (9, 10) to deduce the far field directivity and sound power respectively. These estimates were then compared against direct measurements from the 11 far field measurements.

3.1 Equipment and set-up

A schematic of the experimental set up is shown in Figure 1. A circular duct manufactured from hard plastic of 0.2m internal radius (a) and 4.34m in length (L) was located through the wall separating a reverberation chamber (on the right) and an anechoic chamber (on the left). The sound field transmitted along the duct and subsequently radiated from the open end was generated by 4 high-powered loudspeakers positioned in the corners of the reverberation chamber, driven by independent broadband random signals to generate a broadband diffuse sound field (above the Schroeder frequency). The random sound field impinging on the open of the duct was then transmitted through the duct. Some of this sound field is reflected back into the duct with the rest being radiated into the anechoic chamber on the other side.

The coherence function at the duct wall were measured using two electret microphones separated by a distance Δx, with the distance of the microphone closest to the open end in the source room at a distance x_D, as shown in Figure 1. Eleven ½ inch Bruel and Kjaer microphones were equally spaced along a polar arc between $\theta_i = 0°$ and 100° from the duct axis, at a constant radius R of 2.5m from the end of the duct, were used to measure the directivity and sound power from the duct. The directly measured directivity and sound power were then compared against that predicted based on measurements of the in-duct complex coherence function from Eqs. (7, 8) and (9, 10) respectively.

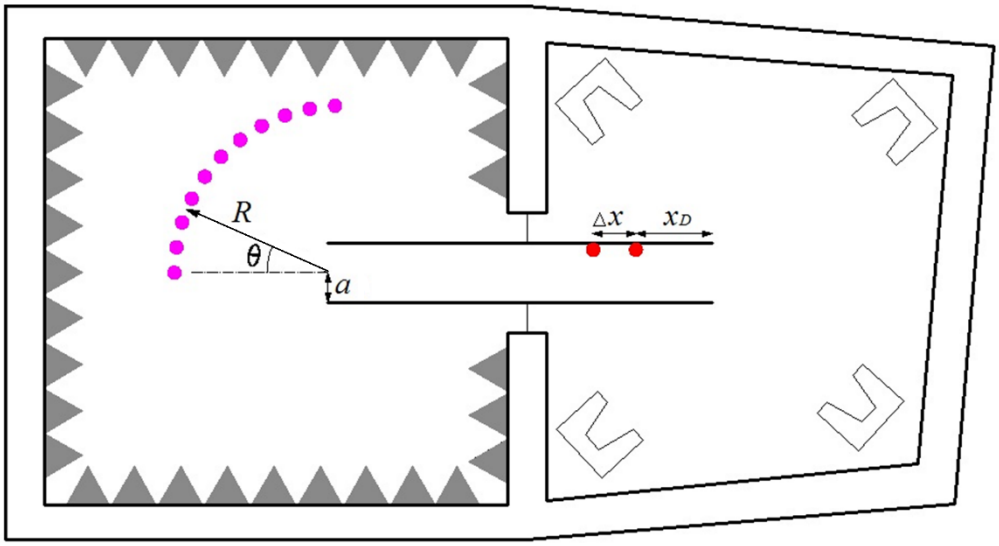

Figure 1: Schematic of the experimental set-up with the duct located between the wall separating the reverberation chamber (left) and anechoic chamber (right). Sources in the reverberation chamber excited the duct which is then measured on the duct wall and in the far field of the anechoic chamber.

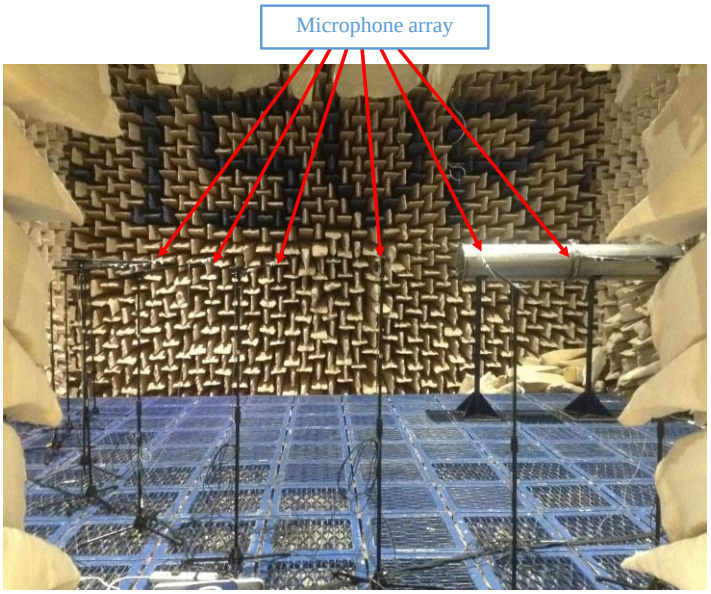

Figure 2: Photograph of the experimental set-up within the large anechoic chamber.

Figure 2 shows the experimental setup within the anechoic chamber. The duct can be seen passing through right hand side wall of the anechoic chamber with the circular array of far-field microphones located at the same height as the duct axis.

Pre-amplification of the in-duct electret microphones and far-field Brüel & Kjaer microphones (red and pink dots respectively in Figure 1 were provided by in-house amplifiers. The loudspeakers were driven by independent random broadband signals produced by four Brüel & Kjaer Type 1405 Noise

Generators. The signal from each generator was passed through separate channels of a Yamaha P2160 power amplifier and out through four separate EV T251+ Trapezoidal Stage System loudspeakers.

In order to ensure that the duct was excited by a diffuse field, the excitation frequency was chosen to be above the Schroeder frequency for the source room calculated from $f_{sch} = 2000\sqrt{T_{60}/V}$, where V = 101.2m^3 is the source room volume and T_{60} is the reverberation time of 0.62s. The corresponding Schroeder frequency for the source room f_{sch} is about 150Hz, which is well below most of the frequency range of interest. Previous work [13] has shown that excitation of the sound field within a duct exited by a diffuse field provides a good approximation to the case where each acoustic mode has identical sound power (the so called, 'equal energy per mode' sound field). In this case the mode amplitudes are predicted to vary as $\overline{a^2}(\alpha) \propto |\alpha|^{-1}, (\alpha \geq 0)$ and the radiation directivity predicted to vary as $S_{ff}(\omega,\theta) \propto \cos\theta$. These predicted results will be compared against the measurements in Section 4.

3.2 Measurement procedure

Acoustic pressure data at the in-duct and far field microphones were acquired simultaneously at a sampling frequency of 50 kHz for a duration of 10s. For a sound field with perfectly uncorrelated mode amplitudes E{ $A_{mn}(\omega)A_{m'n'}(\omega)$ }=0 for $m \neq m', n \neq n'$, Eq. (4a) predicts that the coherence function, and hence inferred mode amplitude distribution function, are independent of the microphone separation distance Δx and position x_D within the duct. To assess the validity of this assumption the in-duct acoustic pressure measurements were made using pairs of microphones at varying distances x_D along the duct and at different separation distances Δx. The location of the microphone pair x_D was varied between x_D =0.5m to x_D =3m with x_D =0 m situated at the source room end of the duct. The separation distance between the microphones was varied between Δx =0.01m and 0.1m in increments of 0.01m.

A number of tests were made to assess the diffuseness of the source room sound field by traversing a microphone around it. Deviations in pressure around the source room were less than about 3dB thereby confirming that it has an acceptable degree of diffuseness. A simple test was also undertaken to assess the degree of modal correlation within the duct by comparing the pressure spectra at a single microphone at various circumferential positions around the duct wall. Deviations in spectra were limited to a few dB, which also confirms the high degree of de-correlation between the mode amplitudes.

3.3 Data analysis methodology

The far field directivity $S_{ff}(\omega,\theta)$ (Pressure PSD versus angle) and radiated sound power spectral density $W(\omega)$ were measured using 11 far-field microphones in the anechoic chamber, as shown in Figure 2. The sound power was calculated assuming axi-symmetry of the sound field and by a discrete integration of the far field intensity given by

$$W(\omega) = 2\pi R^2 \sum_{i=1}^{11} \frac{S_{ff}(\omega,\theta_i)}{\rho c} \sin\theta_i \, \Delta\theta_i \tag{12}$$

where $\Delta\theta_i$ is the angular separation distance between the i^{th} microphone pair.

4. Experiment results and discussion

4.1 Characteristics of the in-duct and far field sound field

Before assessing the accuracy of the two-microphone method for deducing the transmitted sound power and far field directivity, we first assess the characteristics of the in-duct and far field sound field. Figures 3(a) and (b) show simultaneous measurements of the PSD of the acoustic pressure on the duct wall and at the far field microphone at 0° to the duct axis, respectively, plotted against non-dimensional duct-based frequency *ka* up to *ka* = 10. Shown on these figures (as vertical green lines) are the first 10 axial resonance frequencies $f_{Ax,n}$ assuming an open-open pipe where an end correction of 0.6*a* is assumed at each end, and hence are given by $f_{Ax,n} = nc/(L + 2\times 0.6a)$ where *n* is an integer and *L* is the duct length. Also shown on these figures (as vertical red lines) are the first 8 non-dimensional modal cuton frequencies $\kappa_{mn}a$, with the lowest of *ka* = 1.84 delineating the frequency range between purely plane wave propagation, *ka* < 1.84, and higher order modes *ka* > 1.84.

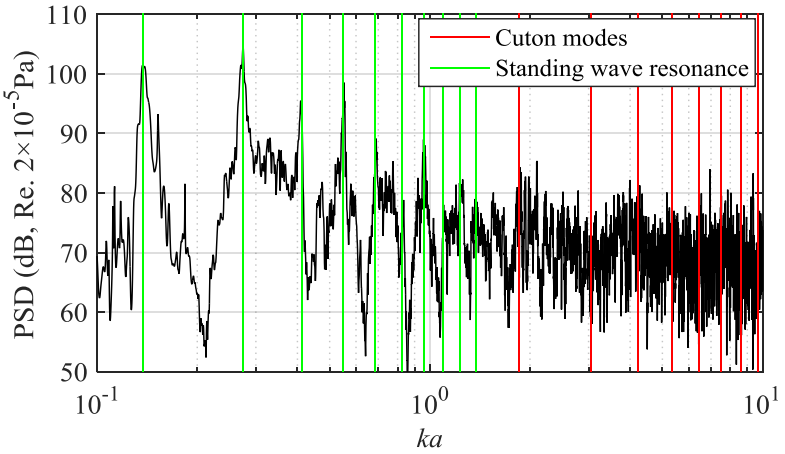

(a) In duct pressure spectrum

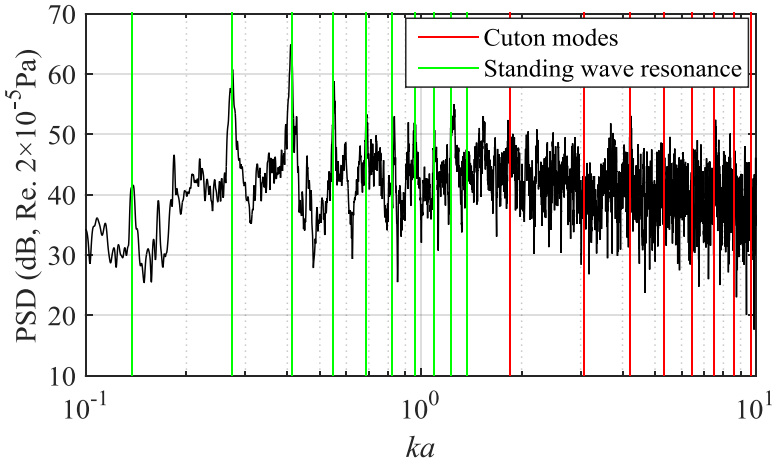

(b) Far field pressure spectrum

Figure 3: Comparison of standing waves and cuton modes in the pressure spectra of in-duct and far-field

Both spectra are observed to be highly oscillatory with a sharp peak occurring in both spectra at the frequencies $f_{Ax,n}$ at which axial resonance occurs. The peaks in the far field spectra in Figure 3(a) also correspond to peaks in the in-duct spectra in Figure 3(b). These frequencies correspond to axial resonance frequencies at which the plane wave amplitude increase to very high levels in both in-duct and far field. Differences in in-duct and far field levels are of course observed at $ka < 0.5$, where the reflection coefficient at the open end is very high. At frequencies above the first cuton frequency $ka = 1.84$, both spectra exhibit considerable levels of oscillation, which is partly due to the very narrow frequency bandwidth used in the analysis to resolve the low frequency spectral peaks. No distinct behaviour can be observed at the modal cuton frequencies indicated by the red lines.

One of the objectives of this paper is to use the two microphone method to deduce the far field radiation from in-duct coherence measurements. Before applying this method to the measured in-duct

pressure data we first assess the relationship between the in-duct and far field pressure spectrum by plotting in Figure 4, and the transmission coefficient $\sigma(\omega, \theta{=}0°)$ defined here as the scaled ratio between the radiated pressure spectrum $S_{ff}(\omega,0)$ at $\theta = 0°$ to the duct axis and the in-duct pressure spectrum $S_{11}(\omega)$ at the duct wall,

$$\sigma(\omega,\theta=0°)=\frac{2R^2 S_{ff}(\omega,\theta=0°)}{a^2 S_{11}(\omega)} \tag{13}$$

which may be interpreted as a non-dimensional efficiency factor between the in-duct pressure spectrum, including reflections, and the far field pressure spectrum.

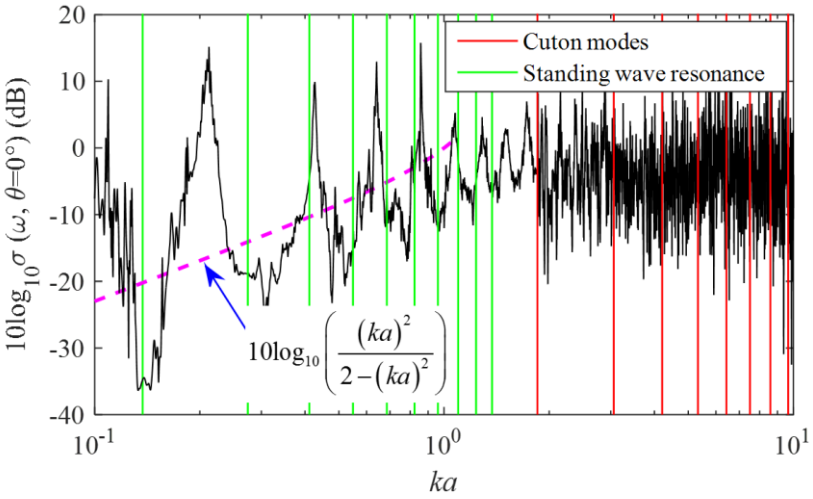

Figure 4: Transmission coefficient $\sigma(\omega, \theta{=}0°)$ versus *ka*

At *ka* values greater than about 1 the scaled ratio oscillates about 0dB. At *ka* less than about 1, the far field pressure spectrum relative to the in-duct pressure spectrum drops sharply. To explain this behaviour consider the spectrum of transmitted sound, which can be expressed in terms of the spectrum of the pressure $S_{ii}(\omega)$ incident upon the open end of the duct and the plane wave energy transmission coefficient $|T(\omega)|^2$ as

$$W(\omega)=\frac{S_{ii}(\omega)}{\rho c}\pi a^2 |T(\omega)|^2 \tag{14}$$

where $|T(\omega)|^2$ is the ratio of pressure PSD incident upon the open end and that transmitted immediately on the other side. The radiated sound power spectrum can also be expressed in terms of the power spectrum of the radiated pressure at the microphone at polar angle $\theta = 0°$ by assuming that

at these low frequencies $ka < 1$, the sound radiates omni-directionally in the forward arc over the area $2\pi R^2$, where R is the distance of the microphone from the duct open end (=2.5m), in the form,

$$W(\omega) = \frac{S_{ff}(\omega,0)}{\rho c} 2\pi R^2 \qquad (ka < 1) \tag{15}$$

A single microphone in the duct detects the sum of the incident and reflected pressure from the end. Neglecting interference between the incident and reflected pressures, the measured pressure PSD in the duct $S_{11}(\omega)$ is related to the incident pressure spectrum by $S_{11}(\omega) = S_{ii}(\omega)\left[1+\left|R_r(\omega)\right|^2\right]$, $\left|R_r(\omega)\right|^2$ is energy reflection coefficient, and therefore $S_{ii}(\omega) = S_{11}(\omega)\Big/\left(1+\left|R_r(\omega)\right|^2\right)$. Combining Equations (14) and (15) gives the following expression for the in-duct to far-field transmission coefficient in terms of $\left|R_r(\omega)\right|^2$ and $\left|T(\omega)\right|^2$,

$$\sigma(\omega) = \left|T(\omega)\right|^2 \Big/ \left[1+\left|R_r(\omega)\right|^2\right] \tag{16}$$

Following Levine and Schwinger [15], the energy transmission coefficient in the frequency limit for a flanged duct is $\left|T(\omega)\right|^2 = (ka)^2$ ($ka < 0.5$) and by energy conservation the energy reflection coefficient equals $\left|R_r(\omega)\right|^2 = 1-(ka)^2$. In the low ka limit, therefore,

$$\sigma(\omega) = (ka)^2 \Big/ \left[2-(ka)^2\right] \tag{17}$$

In Figure 4 the efficiency factor $10\log_{10}\left[\sigma(\omega)\right]$ is plotted as a dashed line for ka values less than 1. This function appears to provide a good approximation to the general behaviour of the far field to in-duct pressure ratio in the low ka limit. At these low frequencies, therefore, most of the sound is reflected back into the duct with comparatively little sound power being radiated to the far field.

4.2 Complex coherence function

The underlying assumption of the two-microphone method is the assumption that the frequency dependent mode amplitude can be written as the product of a purely frequency-dependent source term and a non-dimensional mode amplitude distribution, i.e. $E\left\{\left|A^{\pm}_{mn}(\omega)\right|^2\right\} = S(\omega)\overline{a^2_{\pm}}(\alpha_{mn})$. A consequence of making this assumption is that the complex coherence function is only a function of the non-dimensional frequency $\hat{\omega} = \omega\Delta x / c$, as indicated in Eq. (4a) and explained more fully in Ref. [10]. We now test this assumption on the measured in-duct pressure data by computing the magnitude

and phase of the complex coherence function up to a maximum frequency of 25kHz at the three microphone separation distances of Δx = 0.03, 0.07 and 0.10m located arbitrarily at x_D =1.5m along the duct. The magnitude and phase of the coherence are plotted against $\hat{\omega}$ in Figure 5 (a) and (b) respectively. Note that $ka/\hat{\omega} = a/\Delta x$. Good collapse of the measured coherence magnitude and phase are observed over the frequency range $\hat{\omega} < 14$ where the spectra overlap. The jump in the phase spectrum for Δx = 0.07m in the frequency range $\hat{\omega} > 7$ arise due to 2π phase unwrapping issues. The main assumption made in the measurement technique therefore appears to be valid in the test to within 10% for $\hat{\omega} < 5$ and 20% at high frequencies reasonably valid in this test.

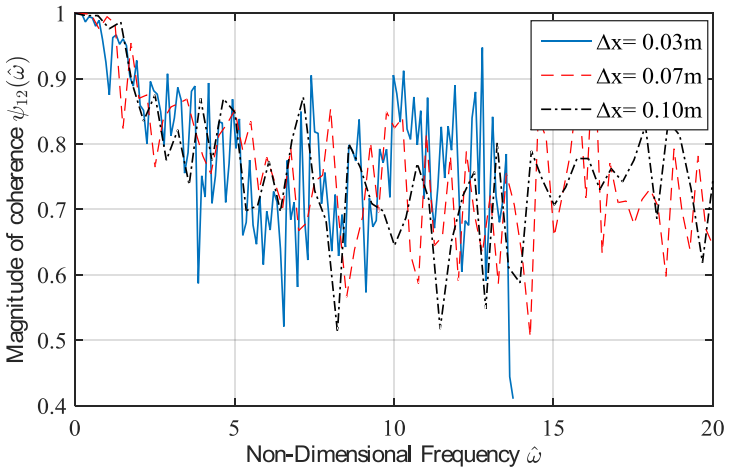

(a) coherence magnitude

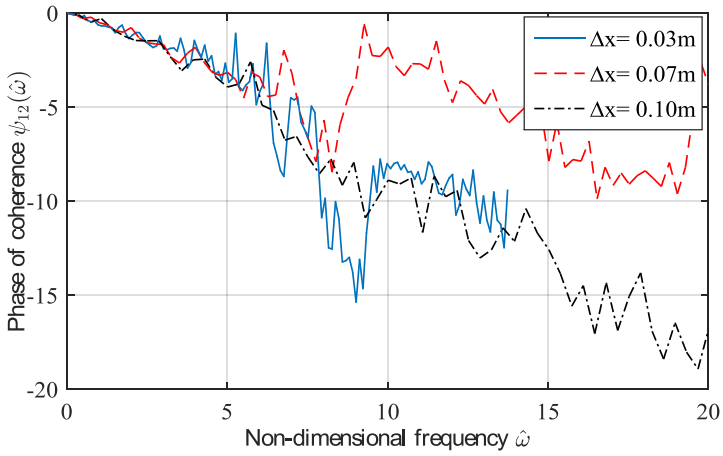

(b) coherence phase

Figure 5: Comparison of the coherence at different microphone separations

A notable feature of Figure 5 (a) is the slow rate of decay of the coherence function with increasing frequency for $\hat{\omega}$ up to about 6. Above this frequency the coherence function remains roughly flat with an average value of about 0.7 over the frequency range shown and beyond. The reason for this behaviour is mostly likely due to the presence of strong axial standing waves in the pipe rig even though the phase spectrum in Figure 5(b) is indicative of waves propagating away from the source.

The coherence measurements presented in Figure 5 were repeated at different positions x_D along the duct and found to have comparatively little effect on the results, and are therefore not shown here.

4.3 Mode amplitude distribution

In this section we use the coherence functions plotted in Figure 5 measured at the three microphone separation distance Δx = 0.03, 0.07 and 0.10m to estimate $\overline{a^2}(\alpha)$ in the duct. The non-dimensional normalised mean square amplitude distribution $\overline{a^2}(\alpha)$ deduced from Eq. (4b) is plotted in Figure 6 (a) versus α for the three separation distances.

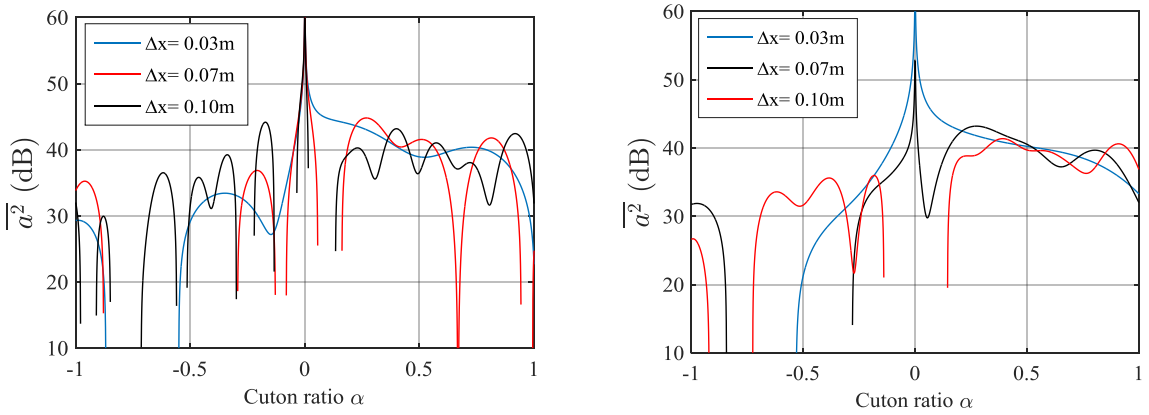

(a) without window function (equivalent to a rectangular window)

(b) with window function

Figure 6: Modal amplitude distribution against the cuton ratio for different microphone separations

In Figure 6 (a) the amplitudes of the modes with positive α, corresponding to the modes propagating away from the source, are typically 10dB above those of the modes propagating in the opposite direction. However, the mode amplitude distribution observed in this figure appears to be rather oscillatory whose peaks and troughs are affected by the microphone separation distance Δx. The reason for these oscillations in the amplitude spectrum is because the magnitude of the coherence function has not sufficiently decayed over the (non-dimensional) frequency range of the measurement.

This upper non-dimensional frequency limit $\hat{\omega}_{max}$ is related to the maximum frequency f_{max} of the frequency spectrum (equal to half the sampling frequency) through $\hat{\omega}_{max} = 2\pi f_{max}\,\Delta x/c$. The separation distance Δx should therefore be sufficiently large to ensure that the coherence function due to the acoustic field has decayed to sufficiently low levels so that it is fully captured by the spectrum.

If the coherence function has not decayed to sufficiently small levels at the maximum frequency $\hat{\omega}_{max}$, as in this case, the Fourier Transform relationship of Eq. (4b) for the mean square mode amplitude distribution becomes strongly influenced by windowing effects so that it may be written in the form,

$$\overline{a^2}(\alpha) = \frac{1}{2\pi|\alpha|}\int_0^{\infty} \Gamma(\hat{\omega})\psi_{12}(\hat{\omega})\mathrm{e}^{-\mathrm{i}\hat{\omega}\alpha}\mathrm{d}\hat{\omega} \qquad (18)$$

where $\Gamma(\hat{\omega})$ is a window function. The oscillations observed in Figure 6 (a) are therefore the result of applying the rectangular window function $\Gamma(\hat{\omega})=1$ for $|\hat{\omega}| < \hat{\omega}_{max}$. To minimize this rectangular windowing effect, $\Gamma(\hat{\omega})$ was replaced by a Hanning window. The Hanning window is one half the Hann function, $\Gamma(\hat{\omega}) = 0.5\left(1-\cos\left(\pi + 2\pi\hat{\omega}/\hat{\omega}_{max}\right)\right)$, $\hat{\omega}$ =[0, $\hat{\omega}_{max}$ /2]. The effect on the three mode amplitude distributions obtained for different Δx by applying the Hanning window in Eq. (18) is shown in Figure 6(b) alongside the mode amplitude distribution estimate obtained without windowing. The mode amplitude spectrum in this Figure6 (b) is much less oscillatory than that in Figure 6 (a).

In Figure 6 (a) and (b), for modes propagating away from the source $\alpha \geq 0$ the estimate of the mode amplitude distribution is reasonably consistent for the three separation distances Δx, with variations being less than about 3dB for α values greater than 0.2. For α values less than 0.2, associated with modes close to cutoff. The estimates deviate considerably more than 3dB. These modes radiate more strongly in the sideline directions. However, the estimate of the mode amplitude distribution for $\alpha < 0$ appears to be highly sensitive to separation distance since these are most strongly affected by the sidelobe behaviour of the window function $\Gamma(\hat{\omega})$.

4.4 Far-field directivity

In this section we compare the far field pressure directivity measurements obtained by the 11 microphones shown in Figure 2 with that obtained from the in-duct coherence measurement in Eq. (8). A comparison of the directly measured far field directivity at the typical frequency of f = 6.6kHz (ka=24.5) with that inferred from the Eq. (8) with Δx = 0.03m is shown in Figure 7 (a). The latter is

shown as the blue solid curve which can be seen to contain a number of spurious side lobes. These are a direct consequence of the rectangular windowing effect discussed in Section 4.3 above.

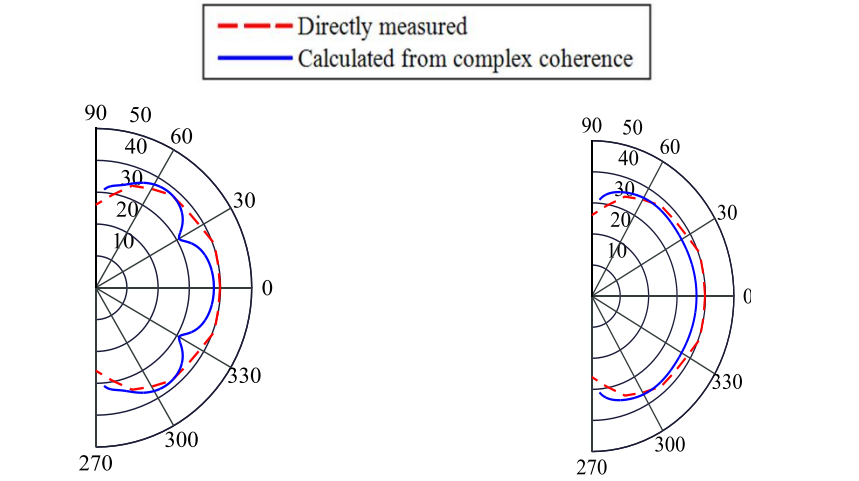

a. without window (equivalent to a rectangular window)

b. with window

Figure 7: Estimated directivity with and without window, at Δx = 0.03m

As for the mode amplitude distribution in Figure 6(a) these spurious oscillations can be largely suppressed by the introduction of a window function $\Gamma(\hat{\omega})$. Eq. (8) for non-dimensional directivity then becomes,

$$d(\theta) = \frac{1}{8\pi}\left(\frac{a}{R}\right)^2 \cos\theta \int_0^\infty \Gamma(\hat{\omega})\psi_{12}(\hat{\omega}) e^{-i\hat{\omega}\cos\theta} d\hat{\omega} \qquad (19)$$

The corresponding directivity estimate obtained using a Hanning window function Γ is shown in Figure 7(b). The spurious oscillations observed with no window function applied in Figure 7(a) are now supressed and the agreement with the measured directivity is much improved.

Further comparisons between the directly measured directivity and that inferred from Eq. (19) is shown in Figure 8 at the three frequencies of 2.875kHz, 6.625kHz and 12.125kHz, representative of the low, middle and high frequency parts of the spectrum, and at the three separation distances of Δx = 0.03m, 0.07m and 0.1m. A consequence of the separability assumption of Eq. (3) is that the normalised directivity $d(\theta)$ function is predicted to be independent of frequency. Comparison of the directly measured directivity functions shown as the red curve in Figure 8, and that from Eq. (19) with Hanning window applied, demonstrates that this conclusion allows for predictions of the far field directivity that is generally within 10dB of the measured directivity, although much better in many

cases (within 5dB). The most significant exception to this conclusion is at the highest frequency f = 12.1kHz where a small peak is observed in the directivity function at about 20° to the duct axis, which is not predicted by the two-microphone method. Agreement between direct and inferred directivity estimate is poorest at the highest frequency f = 12.1kHz.

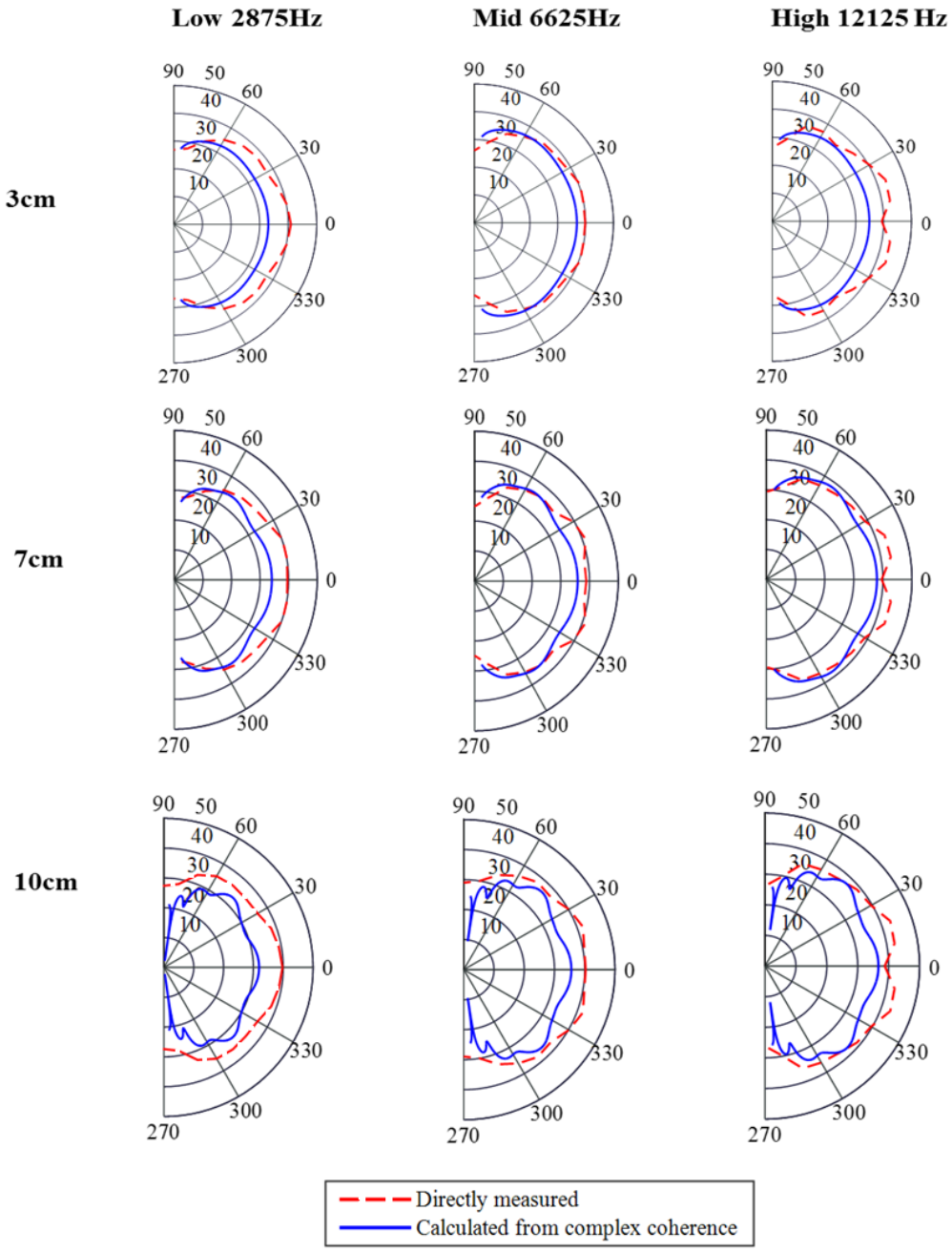

Figure 8: Directivity comparison at different frequencies for different microphone separations

Agreement is also poor at the lowest frequency f = 2.8kHz, corresponding to ka = 10.5 where there are approximately 26 modes propagating. At this frequency, therefore, there may be not sufficient

number of modes to justify approximating the modal sum to an integral. Agreement is poor in the sideline directions for Δx = 0.1m, which is consistent with the high sensitivity of the mode amplitude estimate shown in Figure 6(b) for the near cutoff modes $\alpha \sim 0$, which radiate mostly strongly in the sideline directions, since $\alpha = \cos\theta$.

4.5 Sound power spectrum

In this section we compare in Figure 9 the spectrum of sound power obtained by direct integration of the far field sound intensity (assuming axi-symmetry) in Eq. (12) and that estimated from the coherence function in Eqs. (9 & 10). In order to reveal the low frequency behaviour $ka < 1$ where strong reflections from the open end are observed in Figure 4, the window length for the spectrum estimated was increased to 2^{13} samples corresponding to 0.16s and therefore a frequency resolution of 6.1Hz. However, this increase frequency resolution has led to a highly oscillatory coherence function and therefore spectral density of sound power. The sound power spectra are therefore shown in third octave bands expressed as centre-frequency *ka* values.

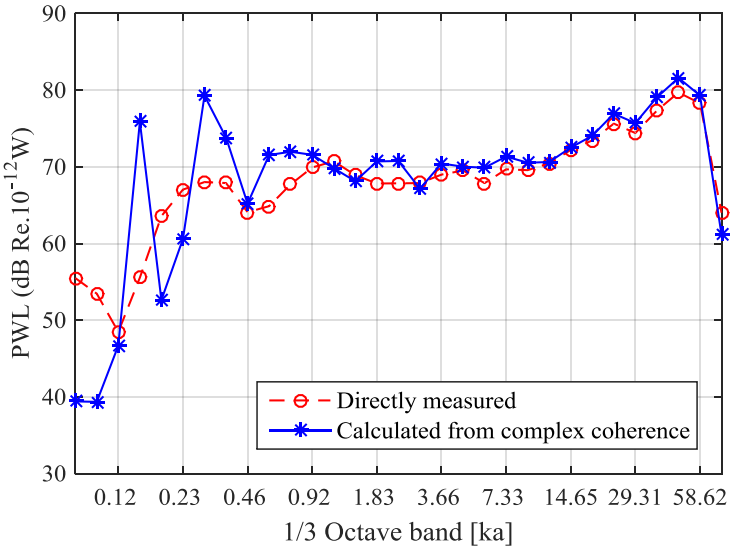

Figure 9: Comparison of the calculated (Δx = 0.07m) and measured far-field sound power PSD

The sound power comparison is generally within about 3dB at *ka* greater than about 10 and within 5dB at *ka* values greater than 1. However at very low frequencies, $ka < 1$, the sound power estimated from the coherence function is significantly over-estimated due to high sound pressure levels $S_{11}(\omega)$ in the duct caused by the high plane wave reflection coefficient at these low frequencies (as shown in Figure 9).

5. Conclusions

This paper describes measurements of the complex coherence function made at two microphones on the wall of a rigid duct excited at one end by a highly reverberant sound field. The coherence function measurements is used in a new measurement method to infer the far field directivity and radiated sound power spectra. These directivity and sound power spectral estimates were compared against the measurements obtained by direct measurements from 11 far-field microphones in an anechoic chamber. The directivity estimates were shown to be within 10dB in all cases and better than 5dB in most cases investigated. Sound power estimates, which is effectively an average value of the directivity estimate, was found to be within 3dB of the directly measured value at frequencies *ka* greater than about 10.

The technique is shown to break down at very low frequencies $ka < 1$ where reflections back into the duct are significant. Agreement is also poorer at *ka* values less than about 10 (where there are less than about 30 propagating modes) where the mode amplitude distribution versus α can no longer be regarded as a continuum and the modal sum replaced by an integral.

In conclusion, therefore, the two microphone method has been validated under laboratory conditions for the case of zero Mach number. Further work is needed to establish the validity of the method for realistic sources, such as fan, and in the presence of a mean flow.

References

[1] Sijtsma P., Feasibility of in-duct beamforming, 13th AIAA/CEAS Aeroacoustics Conference, AIAA-2007-3696, Rome, Italy, 2007.

[2] Dougherty R.P., Mendoza J.M., Nacelle in-duct beamforming using modal steering vectors, 14th AIAA/CEAS Aeroacoustics Conference, AIAA-2008-2812, Vancouver, Canada, 2008.

[3] Lowis C.R., Joseph P., A focused beamformer technique for separating rotor and stator-based broadband sources, 12th AIAA/CEAS Aeroacoustics Conference, AIAA 2006-2520, Cambridge, USA, 2006.

[4] Bolleter U., Crocker M., Theory and measurement of modal spectra in hard-walled cylindrical ducts, Journal of the Acoustical Society of America, 1972; 51:1439–1447.

[5] Ganz U. W., Joppa P. D., Patten T. J. and Scharpf D. F., Boeing 18-inch fan rig broadband noise test. Technical Report CR-1998-208704, NASA, 1998.

[6] Premo J., Joppa P., Fan noise source diagnostic test—wall measured circumferential array mode results, 8th AIAA/CEAS Aeroacoustics Conference, AIAA 2002-2429, Brekenridge, USA, 2002.

[7] Enghardt L., Lowis C. and Neuhaus L., Broadband sound power determination in flow ducts. 10th AIAA/CEAS Aeroacoustics Conference, AIAA-2004-2940, Manchester, UK, 2004.

[8] Enghardt L., Holewa A. and Tapken U. Comparison of different analysis techniques to decompose a broad-band ducted sound field in its mode constituents. 13th AIAA/CEAS Aeroacoustics Conference, AIAA-2007-3520, Rome, Italy, 2007.

[9] Lowis C.R., Joseph P.F. and Kempton A.J., Estimation of the far-field directivity of broadband aeroengine fan noise using an in-duct axial microphone array. J Sound Vib, 2010; 329(19): 3940-3957.

[10] Joseph P.F., A Coherence approach to characterizing broadband sound fields in ducts. In: Proc Internoise 2014; 249: 6054–6062.

[11] Joseph P. F., Mouries F. and Enghardt L., A Two-microphone method for the estimation of the mode amplitude distribution on multimode broadband sound field in finite-length ducts with uniform mean flow. 20th AIAA/CEAS Aeroacoustics Conference, AIAA 2014-2915, Atlanta, USA, 2014.

[12] Rice E. J., Multimodal far-field acoustic radiation pattern using mode cutoff ratio. AIAA J., 1978; 16 (9): 906–911.

[13] Joseph P.F., Morfey C.L. and Lowis C., Multi-mode sound transmission in ducts with flow. J Sound Vib, 2003; 264(3): 523-544.

[14] Rice E.J., Heidmann M.F. and Sofrin T.G., Modal propagation angles in a cylindrical duct with flow and their relation to sound radiation, 17th American Institute of Aeronautics and Astronautics, Aerospace Sciences Meeting, AIAA Paper 79-0183, New Orleans, USA, 1979.

[15] Levine H. and Schwinger J., On the radiation of sound from an unflanged circular pipe. Physical Review, 1948; 73: 383-406.

Appendix: Fourier Transform relationship between mean square mode amplitude distribution and complex coherence function

The acoustic pressure cross spectrum between two points separated axially along the duct wall $\boldsymbol{y}_a = (r = a, \theta)$, where a is the duct radius, at axial distances x_1 and $x_1 + \Delta x$, may written as

$$S_{12}(\omega, \boldsymbol{y}_a, x_1, x_2) = \frac{\pi}{T} \mathrm{E}\left\{ p(\boldsymbol{y}_a, x_1)\, p^*(\boldsymbol{y}_a, x_1 + \Delta x) \right\} \tag{A1}$$

For incoherent excitation of the sound field we treat the mode amplitudes as uncorrelated random variables so that $\mathrm{E}\left\{ A_{mn} A^*_{m'n'} \right\} = 0$ for $m \neq m', n \neq n'$. We further assume that the same mode propagating in opposite directions are also uncorrelated such that $\mathrm{E}\left\{ A^+_{mn}(\omega) A^-_{mn}(\omega)^* \right\} = 0$, consequently based on $p^{\pm}_{mn}(\boldsymbol{y}, x) = \mathrm{e}^{-\mathrm{i}\omega t} A^{\pm}_{mn} \Psi_{mn}(\boldsymbol{y}) \mathrm{e}^{\pm \mathrm{i} \alpha_{mn} k x}$ (Eq. (1)), we can get,

$$S_{12}(\omega, \boldsymbol{y}_a, \Delta x) = \sum_{m,n} \left[\mathrm{E}\left\{ \left| A^+_{mn}(\omega) \right|^2 \right\} e^{+\mathrm{i}\alpha_{mn} k \Delta x} + \mathrm{E}\left\{ \left| A^-_{mn}(\omega) \right|^2 \right\} \mathrm{e}^{-\mathrm{i}\alpha_{mn} k \Delta x} \right] \Psi^2_{mn}(\boldsymbol{y}_a) \tag{A2}$$

Work by Rice [12], and more recent work by Joseph et al. [13], have shown that there are a physically important class of source distributions for which the *relative* mode amplitude distribution is *independent* of frequency and only a function of the cut off ratio α_{mn}. Well known examples include a uniform distribution of monopole sources, axial dipole sources and equal energy per mode [13]. In these, and many other source distributions, we may write (note that this equation is same as Eq. (3)),

$$\mathrm{E}\left\{ \left| A^{\pm}_{mn}(\omega) \right|^2 \right\} = S(\omega) \overline{a^2_{\pm}}(\alpha_{mn}) \tag{A3}$$

where $S(\omega)$ is the frequency-dependent source strength with dimensions of pressure squared per unit frequency and $\overline{a^2_{\pm}}(\alpha_{mn})$ specifies the relative distribution of non-dimensional mean square mode amplitudes, which depends only on α_{mn}. The assumption of the separability of $\mathrm{E}\left\{ \left| A^{\pm}_{mn}(\omega) \right|^2 \right\}$ into a purely frequency–dependent term $S(\omega)$ and a mode distribution term $\overline{a^2_{\pm}}(\alpha_{mn})$ (which controls the

spatial variation of the sound field) is central to the validity of the technique. The split between the two terms is also essentially arbitrary. We define $\overline{a_{\pm}^2}(\alpha_{mn})$ with the normalization property of $\sum_{m,n}\left[\overline{a_{+}^2}(\alpha_{mn})+\overline{a_{-}^2}(\alpha_{mn})\right]=1$. We now denote the amplitude of waves propagating against the direction of flow (i.e., reflected modes in this case) by negative argument α so that (note that this equation is same as Eq. (5))

$$\begin{aligned}\overline{a^2}(\alpha)&=\overline{a_{+}^2}(\alpha) \qquad (\alpha\geq 0)\\ \overline{a^2}(\alpha)&=\overline{a_{-}^2}(-\alpha) \qquad (\alpha\leq 0)\end{aligned} \tag{A4}$$

In the high frequency limit ($ka = \omega a/c > 10$ has been found to be sufficient), we may treat $\overline{a^2}(\alpha)$ as a continuous variable so that the discrete summation over $\overline{a^2}(\alpha_{mn})$ in Eqs. (A2, A3) may be replaced by an integration over α. The normalization condition of $\sum_{m,n}\left[\overline{a_{+}^2}(\alpha_{mn})+\overline{a_{-}^2}(\alpha_{mn})\right]=1$ may therefore be written as $\int_{-1}^{1}\overline{a^2}(\alpha)n(\alpha)\mathrm{d}\alpha=1$, where $n(\alpha)$ the modal density function is introduced to take account the distribution of modes across their range of α- values, defined by,

$$n(\alpha)=\left.\frac{N(\alpha+\delta\alpha)-N(\alpha)}{\mathrm{N}\delta\alpha}\right|_{\lim\delta\alpha\to 0}, \qquad \int_{-1}^{1}n(\alpha)\mathrm{d}\alpha=1 \tag{A5}$$

where $N(\alpha)$ is the number of modes with 'α' values of between -1 and α, and N is the total number of propagating modes at frequency ka, i.e., $\mathrm{N}=\int_{-1}^{1}N(\alpha)\mathrm{d}\alpha$. Rice [12] has shown that in a cylindrical duct with uniform mean flow, the total number of propagating modes N takes the high-frequency limiting value, $\mathrm{N}\to\left(\tfrac{1}{2}ka\right)^2$, $ka\to\infty$. Following Rice [12], and re-expressed in terms of cuton ratio α by Joseph et al. [13], the high-ka asymptotic density function $n(\alpha)$ is given by $n(\alpha)=|\alpha|$, and this equation indicates a scarcity of modes that are just cut-on ($\alpha\approx 0$) compared with a higher population of modes that are well cut on, ($|\alpha|\approx 1$).

Simplifications to Eq. (A2) for the pressure cross spectrum at the duct wall are obtained by replacing $\Psi_{mn}^2(\boldsymbol{y_a})$ by its average value at the duct wall [13], averaged over all values of mode indices m and n,

$$\Psi_{mn}^2\left(\boldsymbol{y_a}\right)=\left\langle\Psi^2\left(\boldsymbol{y_a}\right)\right\rangle_{mn}=2\,. \tag{A6}$$

Taking the average incurs greatest error for modes with the largest *m* values whose values of $\Psi_{mn}^2\left(\boldsymbol{y_a}\right)$ are concentrated at the duct wall. These modes are comparatively scarce, however (with *m* = 0 having the largest number of radial modes and hence being most common), and hence the approximation of Eq. (A6) introduces negligible error compared with the exact calculation of Eq. (A2). Substituting Eq. (A3) for $\left|A_{mn}\left(\omega\right)\right|^2$, and taking the high frequency limit in the sense of $\int_{-1}^{1}\overline{a^2}\left(\alpha\right)n\left(\alpha\right)\mathrm{d}\alpha=1$, leads to an integral expression for the pressure cross spectrum $S_{12}\left(\omega,\boldsymbol{y}_a,\Delta x\right)$ between two microphones separated axially by a distance Δx at the duct wall $\boldsymbol{y}_a=\left(a,\theta\right)$ involving only the cutoff ratio and the frequency-dependent source strength,

$$\frac{S_{12}\left(\hat{\omega},\boldsymbol{y}_a\right)}{S\left(\hat{\omega}\right)}=2\mathrm{N}\int_{-1}^{1}\overline{a^2}\left(\alpha\right)n\left(\alpha\right)\mathrm{e}^{i\hat{\omega}\alpha}\mathrm{d}\alpha\,, \tag{A7}$$

which is a function only of the non-dimensional frequency, $\hat{\omega}$

$$\hat{\omega}=\omega\Delta x/c \tag{A8}$$

Note that the source term $S=S\left(\hat{\omega}\right)$ has also been written as a function of $\hat{\omega}$ which is permissible since *S* is a source term and therefore unrelated to Δx and so there is no difficulty in non-dimensionalising the source frequency ω with respect to this arbitrary distance.

A consequence of making the separability assumption of Eq. (A3) is that the cross spectrum is only a function of the non-dimensional frequency $\hat{\omega}$. Thus, cross spectra measured at the duct wall for different separation distances Δx, plotted against $\hat{\omega}$, should collapse provided that this separability assumption is met. This property therefore provides a simple test of the validity of Eq. (A3). In practice, however, the coherence measurement will be affected by non-acoustic pressure contributions from flow noise at the microphones. In practice, therefore, steps should be taken to minimize contamination by flow noise by, for example, recessing the microphones into the duct wall.

Moreover, the source strength $S\left(\hat{\omega}\right)$ can be interpreted as the high frequency noise pressure spectrum averaged over the duct cross sectional area, per mode. Joseph et al. [13] has shown that, in the high frequency limit, the pressure PSD averaged over the duct cross section, $\mathrm{NS}\left(\hat{\omega}\right)$, is half the pressure

Power Spectral Density (PSD) measured at the duct wall $S_{11}(\hat{\omega},\boldsymbol{y}_a)$, i.e., $S_{11}(\hat{\omega},\boldsymbol{y}_a)=2\mathrm{N}S(\hat{\omega})$, and substituting this into (A7) leads to,

$$S_{12}(\hat{\omega})=S_{11}(\hat{\omega})\int_{-1}^{1}\overline{a^2}(\alpha)|\alpha|\mathrm{e}^{\mathrm{i}\hat{\omega}\alpha}\mathrm{d}\alpha \tag{A9}$$

In Eq. (A9), and all future results, the dependence on $\boldsymbol{y}_a$ is dropped since it is now understood that *all* measurements are made at the duct wall.

Finally we make the approximation that $S_{11}(\hat{\omega})\approx S_{22}(\hat{\omega})$ and hence $S_{11}(\hat{\omega})\approx\sqrt{S_{11}(\hat{\omega})S_{22}(\hat{\omega})}$, since Δx is usually very small (typically a few centimeters), and set the upper limit of integration to infinity (since $\overline{a^2}(\alpha)\approx 0$ for $|\alpha|>1$ corresponding to cutoff modes). The final result is,

$$\psi_{12}(\hat{\omega})=\int_{-\infty}^{\infty}\overline{a^2}(\alpha)\,|\alpha|\mathrm{e}^{\mathrm{i}\hat{\omega}\alpha}\mathrm{d}\alpha \tag{A10}$$

Equation (A10) represents a Fourier Transform relationship between α– weighted normalized mode amplitude distribution function $\overline{a^2}(\alpha)$ and the complex coherence function $\psi_{12}(\hat{\omega})\approx S_{12}(\hat{\omega})\big/\sqrt{S_{11}(\hat{\omega})S_{22}(\hat{\omega})}$, ($0\le|\psi_{12}(\hat{\omega})|^2\le 1$). The mean square mode amplitude distribution, with the normalization property of $\sum_{m,n}\left[\overline{a_+^2}(\alpha_{mn})+\overline{a_-^2}(\alpha_{mn})\right]=1$, may therefore be readily deduced from the inverse Fourier Transform of the complex coherence function.

$$\overline{a^2}(\alpha)=\frac{1}{2\pi|\alpha|}\int_{-\infty}^{\infty}\psi_{12}(\hat{\omega})\,\mathrm{e}^{-\mathrm{i}\hat{\omega}\alpha}\mathrm{d}\hat{\omega} \tag{A11}$$